

Supporting Information

Electrodeposited Sn-Cu@Sn dendrites for selective electrochemical CO₂ reduction to formic acid

Jinkyu Lim,^{*a,b} Angel T. Garcia-Esparza,^c Jae Won Lee,^a Gihun Kang,^a Sangyong Shin,^a Sun Seo Jeon^a and Hyunjoo Lee^{*a}

^a Department of Chemical and Biomolecular Engineering, Korea Advanced Institute of Science and Technology, Daejeon 34141, South Korea

^b Linac Coherent Light Source, SLAC National Accelerator Laboratory, Menlo Park, California 94025, United States

^c Stanford Synchrotron Radiation Lightsource, SLAC National Accelerator Laboratory, Menlo Park, California 94025, United States

Additional Data;

Fig. S1-S15

Table S1

References

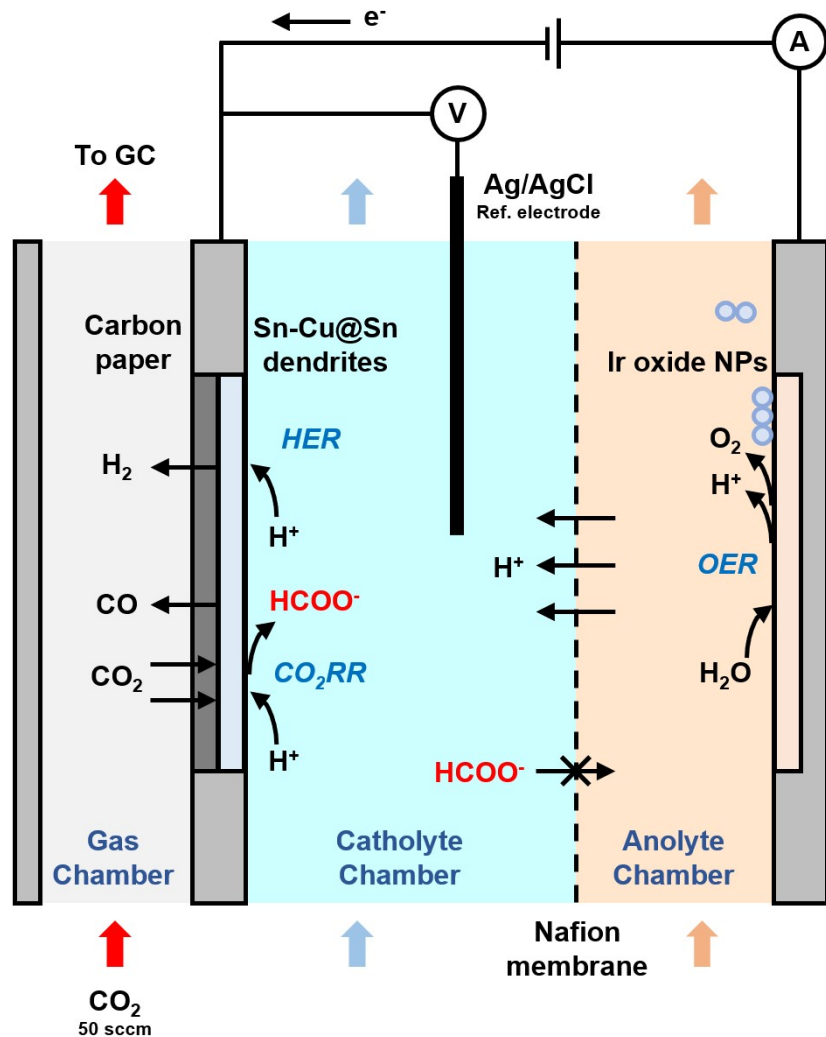


Fig. S1 A scheme of CO_2 electrolysis cell used in this work. The cathode was a gas diffusion electrode (GDE).



Fig. S2 A working electrode for the electrodeposition of Sn-Cu@Sn dendrites. To get uniform result over the whole area, every side of the carbon cloth was covered with epoxy adhesive. Back side of the electrodes were coated by PTFE to avoid contact with the plating solution.

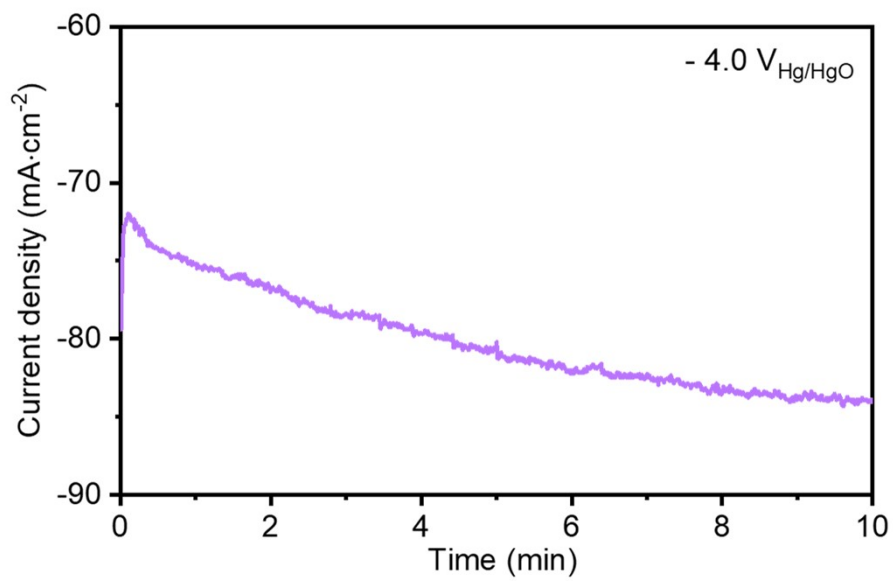


Fig. S3 Transient response of the current density during the electrodeposition of Sn-Cu@Sn dendrites. With the Sn-Cu plating solution, a constant potential of $-4.0 \text{ V}_{\text{Hg}/\text{HgO}}$ was applied for 10 min. Temperature of the plating solution was controlled to be $25 \text{ }^{\circ}\text{C}$ using a water bath.

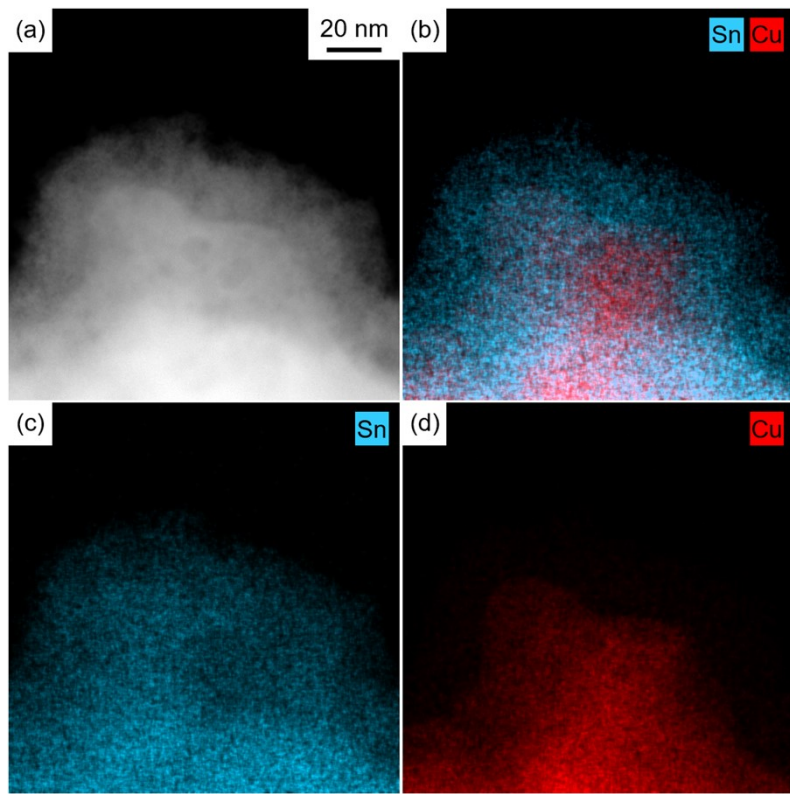


Fig. S4 High resolution (HR) TEM analysis for the Sn-Cu@Sn dendrites. (a) A high angle annular dark field (HAADF) STEM image. (b) Corresponding EDS overlay map and individual maps for (c) Sn, and (d) Cu.

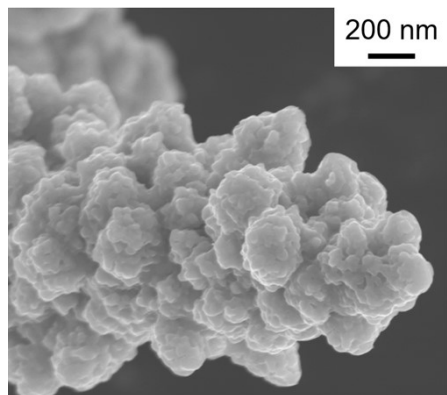


Fig. S5 A high-resolution (HR) SEM image of the Sn-Cu@Sn dendrites

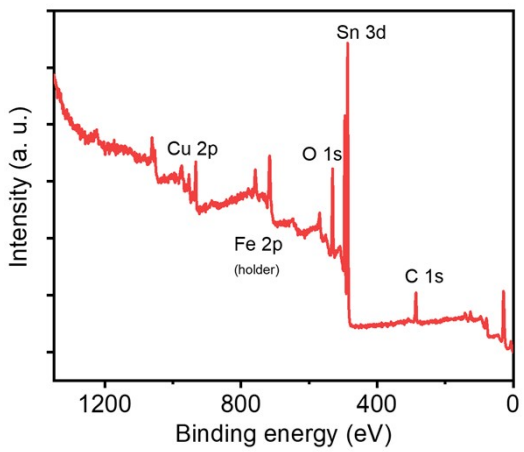


Fig. S6 XPS overall survey spectrum of the Sn-Cu@Sn dendrites.

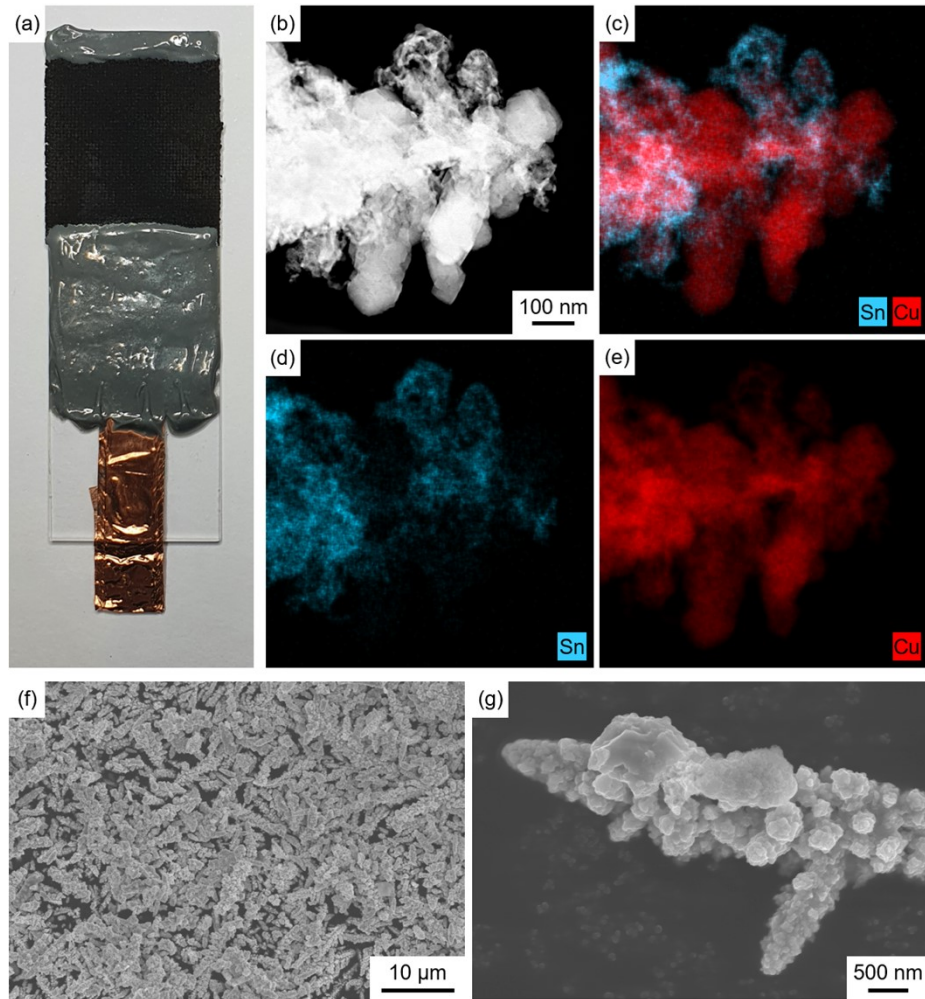


Fig. S7 (a) A working electrode used for the electrodeposition, in which the carbon cloth was not covered with epoxy adhesive completely. (b) A high-resolution HAADF-STEM image for the Sn-Cu catalysts prepared from the working electrode shown in (a). Corresponding EDS mapping results; (c) overlay image, (d) Sn element distribution, and (e) Cu element distribution. (f) A SEM image and (g) a high-resolution SEM image for the poorly shape-controlled Sn-Cu catalysts.

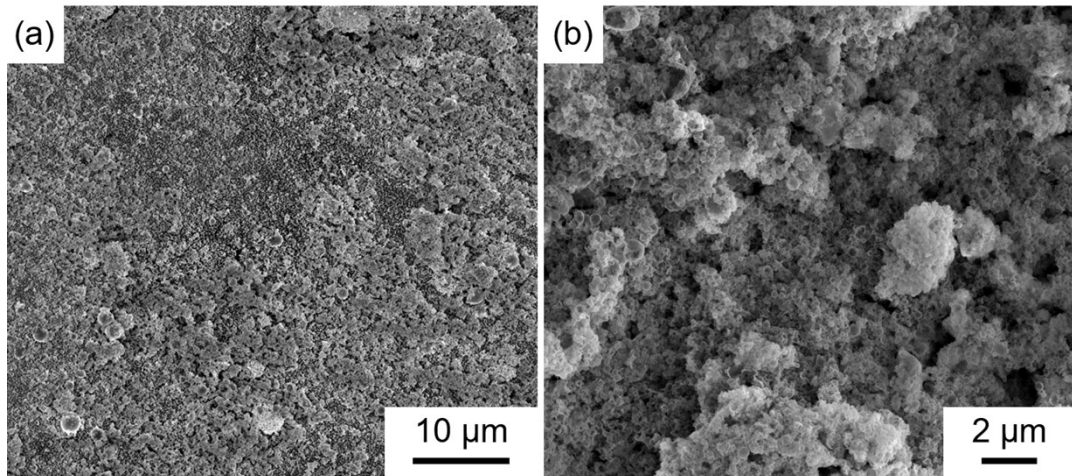


Fig. S8 SEM images of SnNP electrode in different magnifications. Commercial SnNP was deposited on a carbon paper (Sigracet 39 BB). Nafion ionomers bound the particles on the substrate surface.

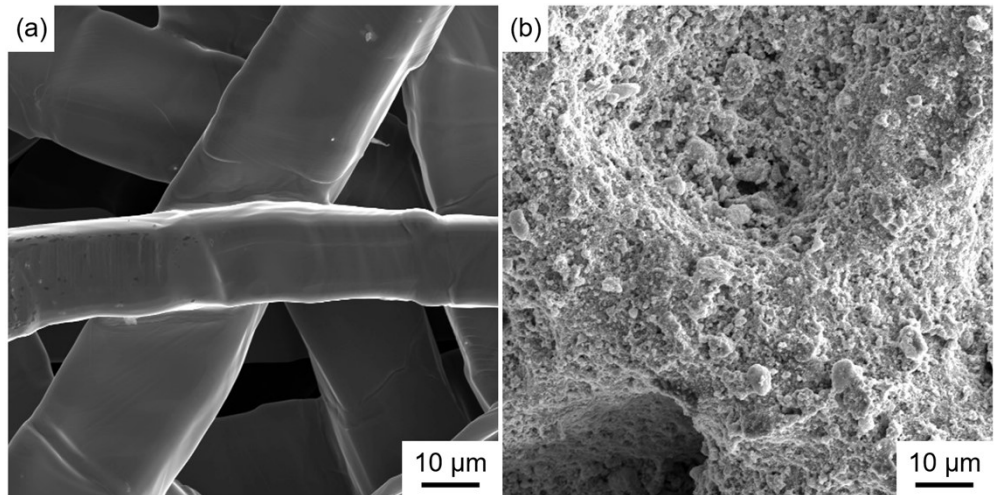


Fig. S9 SEM images of (a) a roll-pressed bare Ti diffusion layer (DL) and (b) the Ti DL with commercial Ir oxide nanoparticles deposited. The electrode shown in (b) was used as an anode for CO₂RR.

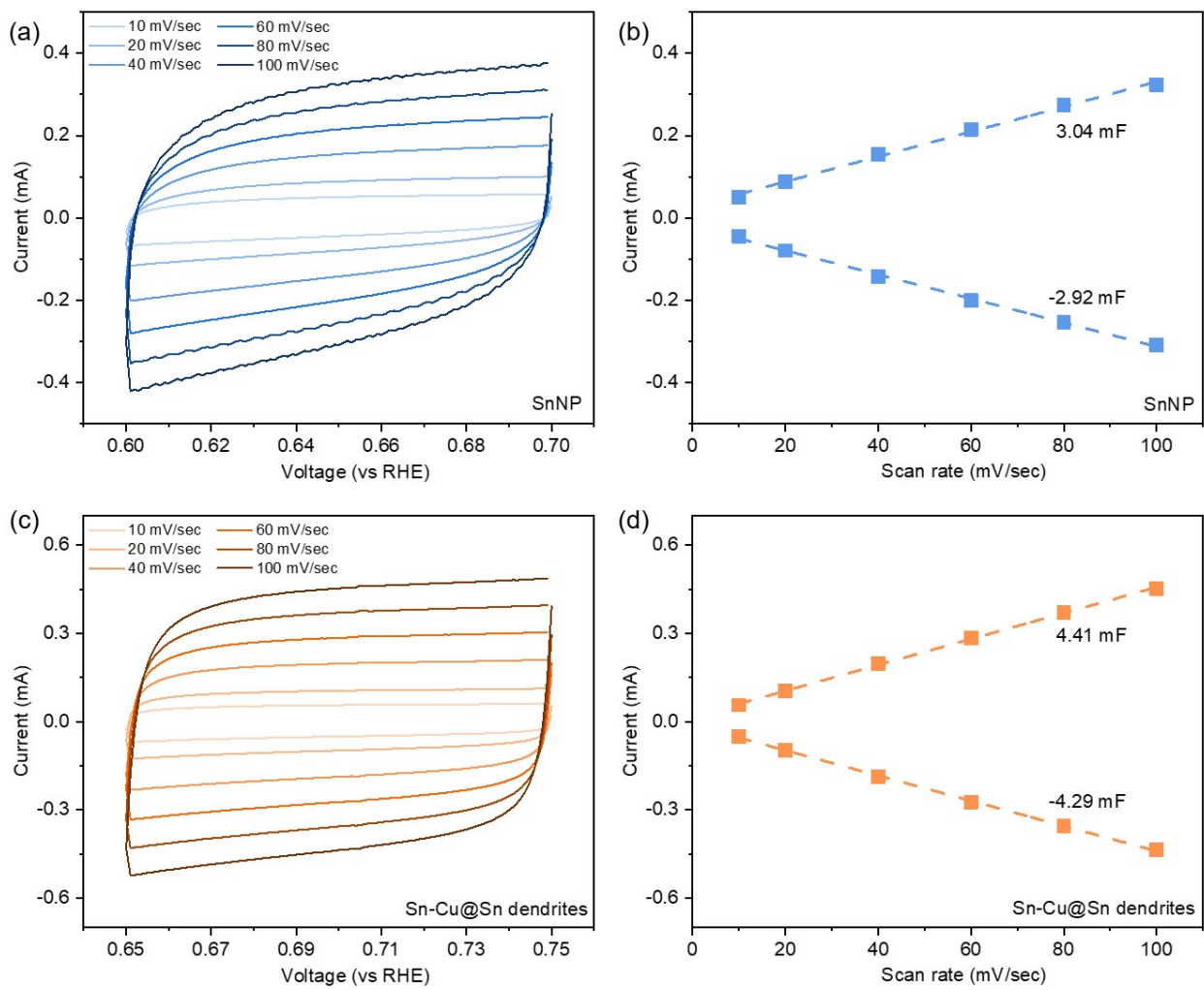


Fig. S10 Measuring double layer capacitances to estimate ECSAs (a), (b) for SnNP and (c), (d) for Sn-Cu@Sn dendrites. CO₂-saturated 1M KHCO₃, a graphite sheet counter electrode, and an Ag/AgCl (3M NaCl) reference electrode were used. The geometric area of the electrodes was 4 cm².

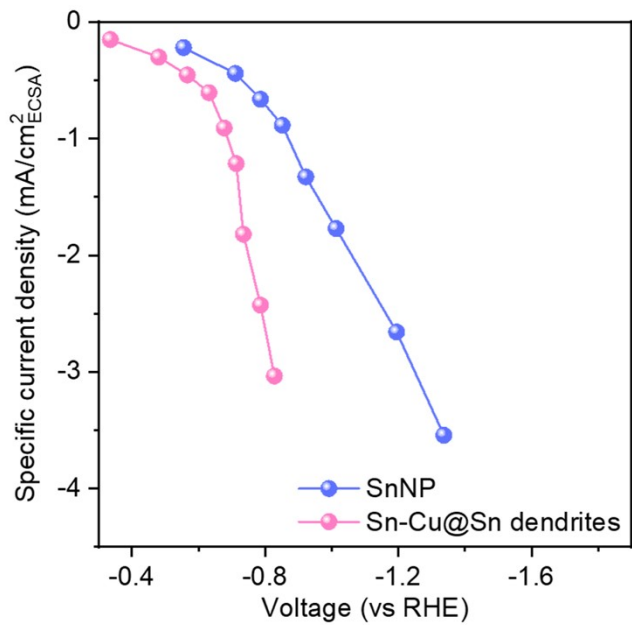


Fig. S11 Specific current densities at various applied potentials. The ECSA of each electrode was 131.8 cm² and 90.3 cm² for Sn-Cu@Sn dendrites and SnNP, respectively. Measurement conditions: 4 cm² GDE, 1.0 M KHCO_{3(aq)}, Ir oxide nanoparticles on pressed Ti DL as anode, Nafion 212 membrane, 25 °C.

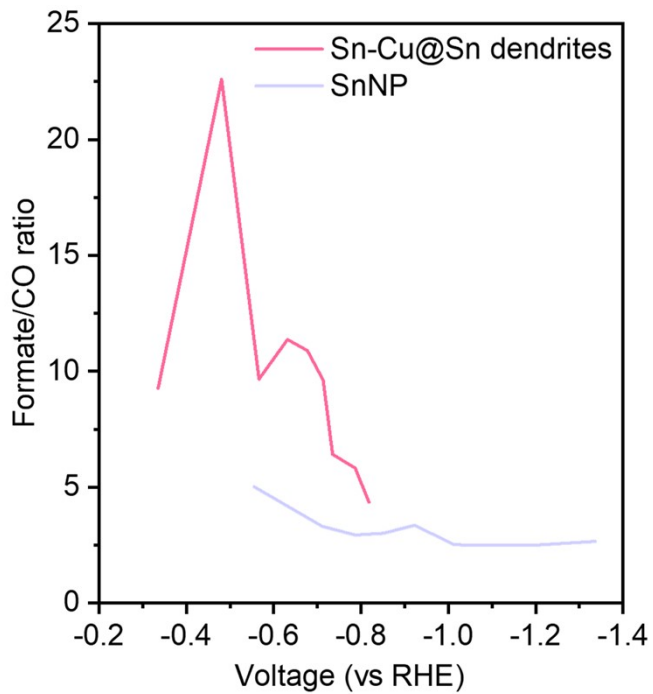


Fig. S12 Selectivity ratios between formate and CO for Sn-Cu@Sn dendrites and SnNP catalysts.

Measurement conditions: 4 cm² GDE, 1.0 M KHCO_{3(aq)}, Ir oxide nanoparticles on pressed Ti DL as anode, Nafion 212 membrane, 25 °C.

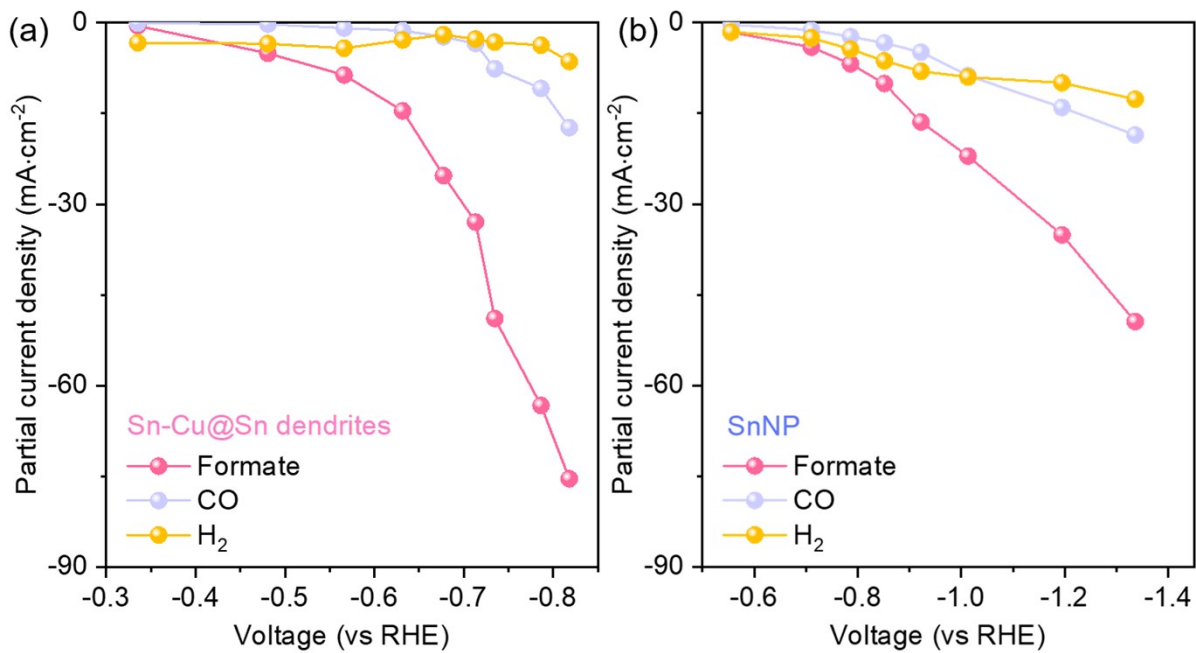


Fig. S13 Partial current densities to formate, CO, and H_2 on (a) Sn-Cu@Sn dendrites and (b) SnNP electrodes. Measurement conditions: 4 cm^2 GDE, 1.0 M $\text{KHCO}_3\text{(aq)}$, Ir oxide nanoparticles on pressed Ti DL as anode, Nafion 212 membrane, 25 °C.

Table S1 Comparison of the CO₂RR to formic acid performance with previously reported catalysts in literatures.

Catalysts	Current density (mA·cm ⁻²)	FE to formic acid (%)	Voltage (V _{RHE})	Electrode type	Electrode size (cm ²)	Ref.
Sn-Cu@Sn dendrites	-30	84.2	-0.68	GDE	4	This work
Sn-Cu@Sn dendrites	-100	75.4	-0.82	GDE	4	This work
Electrodeposited Sn with dense tips	-30	62.5	-0.76	GDE	4	[1]
Sn nanoparticles with Nafion	-13.45	73	-1.2	GDE	7	[2]
Rolling Sn nanoparticles	-22.2	78.60	-1.2	GDE	7	[3]
Sn nanoparticles with PTFE	-22	86.75	-1.2	GDE	7	[4]
Sn powders with Nafion	-27	70	-1.2	GDE	1	[5]
Hierarchical SnO ₂ microsphere	-12.5	62	-1.3	GDE	4	[6]
Sn nanoparticles on carbon	-150	70.2	-0.9	GDE	1	[7]
SnO ₂ nanoparticles	-147	97	-0.95	GDE	0.01	[8]
Electrodeposited Sn	-5	70	-1.6 (vs anode) -2.1 V (vs anode)	GDE	9	[9]
Sn particles	-41.7	95		GDE	25	[10]
Ni doped SnS ₂ nanosheets	-18.5	80	-0.9	Planar	0.5	[11]
Cu-SnO ₂ core-shell/C	-10	93	-0.7	Planar	0.49	[12]
AgSn/SnO _x core-shell	-19	81	-0.8	Planar	0.5	[13]
Pd-B/C	-8	70	-0.5	Planar	0.2	[14]
Bi-Sn bimetallic alloy	-57	94	-1.14	Planar	1	[15]
Hierarchical Sn dendrites	-35	71.6	-1.36	Planar	0.13	[16]
SnO ₂ quantum wires	-16	87	-1.15	Planar	0.785	[17]
Hierarchical mesoporous SnO ₂ nanosheets	-48	88	-1.0	Planar	3	[18]
Reduced SnO ₂ porous nanowires	-8.5	80	-0.8	Planar	5	[19]
Ultra small SnO nanoparticles	-30	67	-0.87	Planar	1	[20]
S doped Sn/Au needles	-55	93	-0.75	Planar	1	[21]

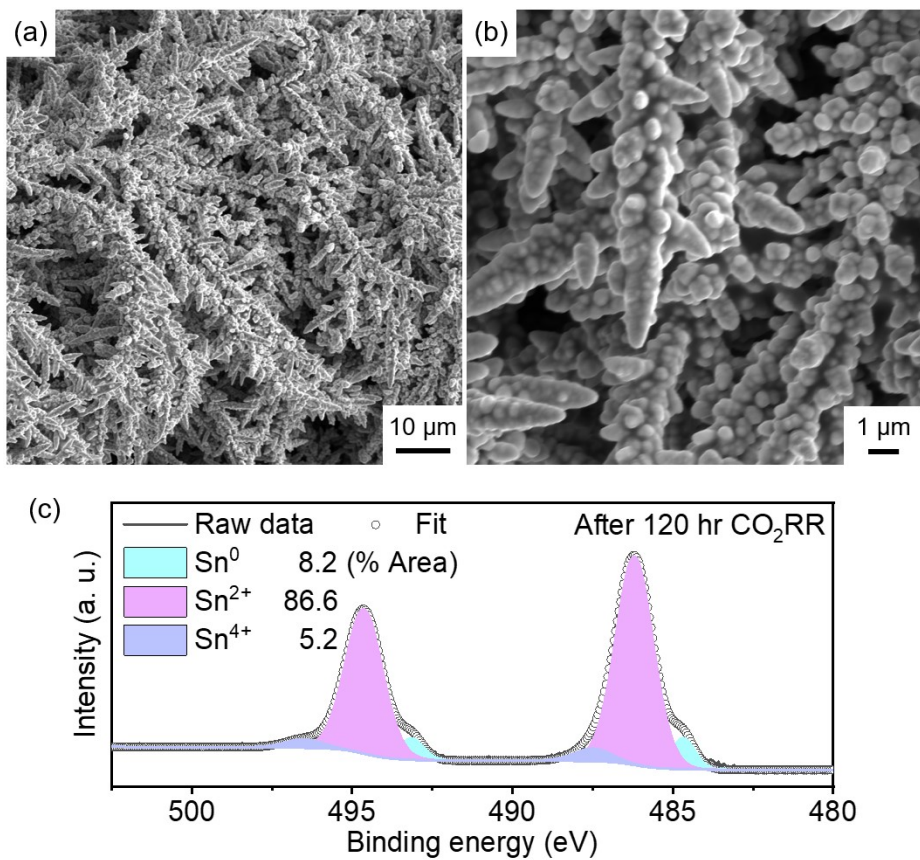


Fig. S14 (a), (b) SEM images and (b) XPS spectrum for the Sn-Cu@Sn dendrites after prolonged CO_2 reduction for 120 hr. The XPS spectrum was convoluted following the same protocol described in the manuscript.

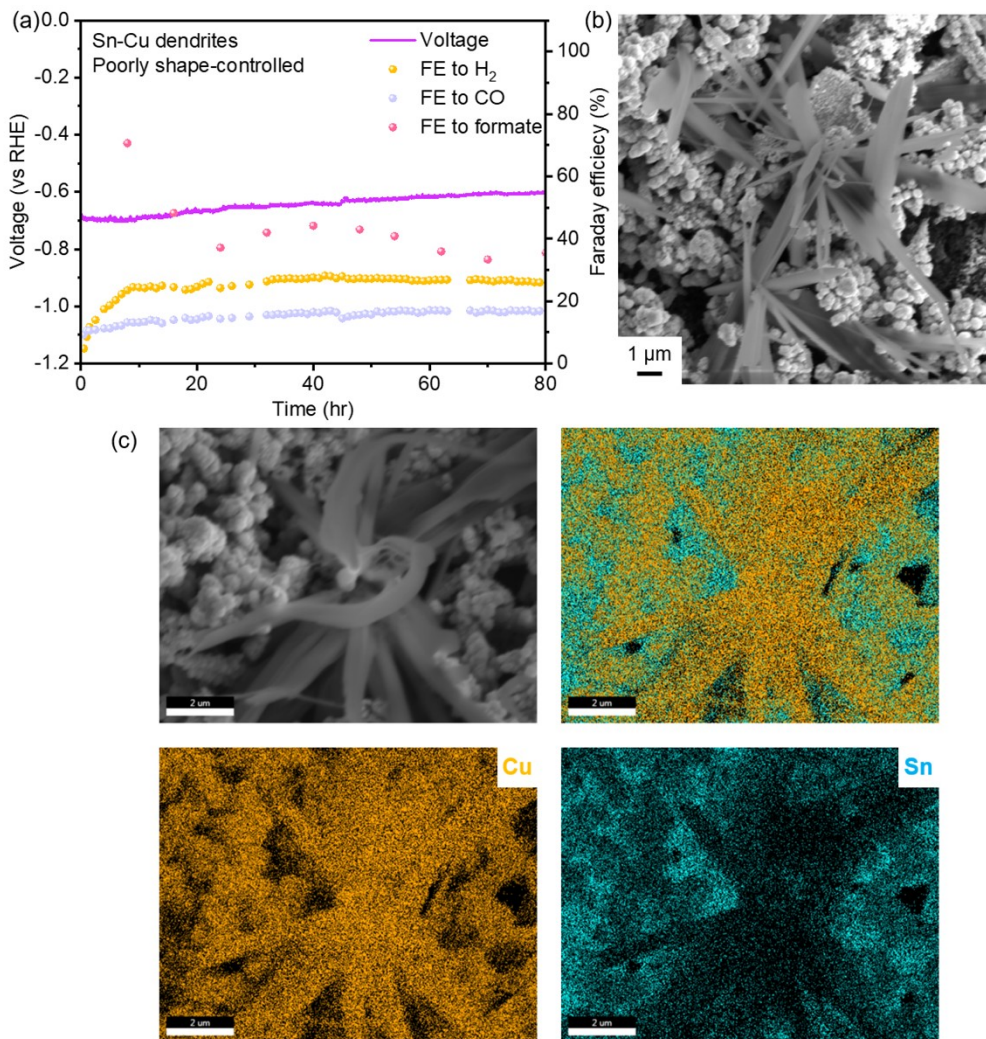


Fig. S15 (a) Prolonged CO₂ electrolysis with poorly shape-controlled Sn-Cu@Sn dendrites. (b) A SEM image of the poorly shape-controlled Sn-Cu@Sn dendrites after the 80 hr electrolysis. Cu nanowhiskers were observed on the surface. (c) SEM-EDS mapping result showing the distribution of Cu and Sn. Measurement conditions: 4 cm² GDE, 1.0 M KHCO_{3(aq)}, Ir oxide nanoparticles on pressed Ti DL as anode, Nafion 212 membrane, 25 °C.

References

- [1] J. Lim, P. W. Kang, S. S. Jeon, H. Lee, *J. Mater. Chem. A* **2020**, 8, 9032-9038.
- [2] Q. Wang, H. Dong, H. Yu, *RSC Adv.* **2014**, 4, 59970-59976.
- [3] Q. Wang, H. Dong, H. Yu, *J. Power Sources* **2014**, 271, 278-284.
- [4] Q. Wang, H. Dong, H. Yu, H. Yu, *J. Power Sources* **2015**, 279, 1-5.
- [5] G. K. S. Prakash, F. A. Viva, G. A. Olah, *J. Power Sources* **2013**, 223, 68-73.
- [6] Y. Fu, Y. Li, X. Zhang, Y. Liu, J. Qiao, J. Zhang, D. P. Wilkinson, *Appl. Energy* **2016**, 175, 536-544.
- [7] A. Del Castillo, M. Alvarez-Guerra, J. Solla-Gullón, A. Sáez, V. Montiel, A. Irabien, *J. CO₂ Util.* **2017**, 18, 222-228.
- [8] C. Liang, B. Kim, S. Yang, L. Yang, C. Francisco Woellner, Z. Li, R. Vajtai, W. Yang, J. Wu, P. J. A. Kenis, Pulickel M. Ajayan, *J. Mater. Chem. A* **2018**, 6, 10313-10319.
- [9] R. L. Machunda, H. Ju, J. Lee, *Curr. Appl. Phys.* **2011**, 11, 986-988.
- [10] W. Lee, Y. E. Kim, M. H. Youn, S. K. Jeong, K. T. Park, *Angew. Chem. Int. Ed.* **2018**, 57, 6883-6887.
- [11] A. Zhang, R. He, H. Li, Y. Chen, T. Kong, K. Li, H. Ju, J. Zhu, W. Zhu, J. Zeng, *Angew. Chem. Int. Ed.* **2018**, 57, 10954-10958.
- [12] Q. Li, J. Fu, W. Zhu, Z. Chen, B. Shen, L. Wu, Z. Xi, T. Wang, G. Lu, J.-j. Zhu, S. Sun, *J. Am. Chem. Soc.* **2017**, 139, 4290-4293.
- [13] W. Luc, C. Collins, S. Wang, H. Xin, K. He, Y. Kang, F. Jiao, *J. Am. Chem. Soc.* **2017**, 139, 1885-1893.
- [14] B. Jiang, X.-G. Zhang, K. Jiang, D.-Y. Wu, W.-B. Cai, *J. Am. Chem. Soc.* **2018**, 140, 2880-2889.
- [15] G. Wen, D. U. Lee, B. Ren, F. M. Hassan, G. Jiang, Z. P. Cano, J. Gostick, E. Croiset, Z. Bai, L. Yang, Z. Chen, *Adv. Energy Mater.* **2018**, 8, 1802427.
- [16] D. H. Won, C. H. Choi, J. Chung, M. W. Chung, E.-H. Kim, S. I. Woo, *ChemSusChem* **2015**, 8, 3092-3098.
- [17] S. Liu, J. Xiao, X. F. Lu, J. Wang, X. Wang, X. W. Lou, *Angew. Chem. Int. Ed.* **2019**, 58, 8499-8503.
- [18] F. Li, L. Chen, G. P. Knowles, D. R. MacFarlane, J. Zhang, *Angew. Chem. Int. Ed.* **2017**, 56, 505-509.
- [19] B. Kumar, V. Atla, J. P. Brian, S. Kumari, T. Q. Nguyen, M. Sunkara, J. M. Spurgeon, *Angew. Chem. Int. Ed.* **2017**, 56, 3645-3649.
- [20] J. Gu, F. Héroguel, J. Luterbacher, X. Hu, *Angew. Chem. Int. Ed.* **2018**, 57, 2943-2947.
- [21] X. Zheng, P. De Luna, F. P. García de Arquer, B. Zhang, N. Becknell, M. B. Ross, Y. Li, M. N. Banis, Y. Li, M. Liu, O. Voznyy, C. T. Dinh, T. Zhuang, P. Stadler, Y. Cui, X. Du, P. Yang, E. H. Sargent, *Joule* **2017**, 1, 794-805.